Open-File Report of Geological Survey of Japan, AIST, no. 735

Petrographic texture of quartz in the Kakkonda granite, northeast Japan

SASAKI Munetake[1] *, SAWAKI Takayuki[1],
FUJIMOTO, Koichiro[1 2] and SASADA, Masakatsu[1 3]

[1] AIST, Geological Survey of Japan, 1-1-1, Higashi, Tsukuba, Ibaraki, 305-8567 Japan.

[2] present address: Tokyo Gakugei University, 4-1-1, Nukuikita-machi, Koganei, Tokyo, 184-8501.

[3] present address: Geo-Heat Promotion Association of Japan, Pacific Arc Building, 5-29-20, Ogikubo, Suginami-ku, Tokyo, 167-0051, Japan.

* corresponding author: sasaki-munetake@aist.go.jp

Key words: quartz, cathodoluminescence, crystal size distribution, solidification of magma, Kakkonda geothermal system, northeast Japan

Abstract

The Kakkonda Granite, regarded as the heat source of the active high-temperature geothermal system at the Kakkonda geothermal field, northeast Japan, was available for the investigation of solidification process of a granitic magma chamber emplaced at a shallow level in the crust. The granitic rocks sampled by the deep geothermal research well WD-1a at high formation temperatures were petrographically examined in this study. The rocks exhibited the porphyritic to equigranular texture at shallow to deep depths. Nucleation and growth rates of plagioclase and quartz crystals in the rocks, determined according to the crystal size distribution theory, became to be slow with depth. Theses petrographic features were attributed to the increase in solidification duration of magma from the margin inward the granitic body, based on a numerical simulation of magma cooling in this study. Cathodoluminescence observation of the granitic rocks revealed crystal growth of quartz at three stages, implying that the magma was not so stable but interactive with respect to quartz, especially at the end during the solidification of magma. Quartz exhibited many branched and curved lines under the cathodoluminescence observation. They were the healed microfractures. The microfracturing of quartz possibly occurred with a relation to the formation of thermal conduction zone with a steep thermal gradient inside the granitic body. It might sporadically provide a pathway for heat and fluid transfer in the granitic body in a geological time. The result of this study might be helpful for a better understanding of the solidification process of the magma and modification of the sequential granite from a petrographic point of view.

1. Introduction

Solidifying magma chamber conceptually consists of the immobile rigid crust, highly viscous mush, and magma-convective suspension from its margin inward based on the rheology and crystallinity (Marsh, 1989; 1996). The solidification front generally moves inward upon cooling, leaving behind the various petrographic texture and mineralogy in the rigid crust with dependence on the temperature, pressure, and degree of liquid-crystal separation. The cooling rate of magma chamber also affects the petrographic texture: with only heat conduction, with magma convection, and with formation of hydrothermal convection at the shallow levels in the rigid crust. Granite is a kind of the immobile rigid crust. It is a potential heat source of the active geothermal system, where the magma chamber is emplaced at a shallow level in the crust.

In the Kakkonda geothermal field, northeast Japan, the deep-seated Kakkonda granite as a heat-source of the geothermal system was discovered at a shallow level (>2,860m depth: Doi *et al*., 1998). A deep geothermal research well WD-1a was drilled into the granitic body (Uchida *et al*., 1996; Muraoka *et al*., 1998), and collected three spot core samples of the granitic rocks at temperatures of 370 to >500 °C (Ikeuchi *et al*., 1998; Saito *et al*., 1998). The rocks preserved the petrographic feature of the high-temperature granite just after solidification of magma (Doi *et al*., 1998; Sasaki *et al*., 2003; Nakano *et al*., 2014).

Quartz is one of the major constituent minerals in granite. It is chemically simple and relatively stable without any growth and alteration texture. However, cathodoluminescence (CL) makes it possible to detect the internal texture of quartz that is invisible to the traditional petrographic techniques (Marshall, 1988; Walker and Burley, 1991; D'Lemos *et al*., 1997; Seyedolali *et al*., 1997; Yuguchi *et al*., 2020). The method might provide new insights into petrographic feature of granite. Crystal

size distribution (CSD) of the constituent minerals in granite including quartz is also available for the examination of petrographic feature of granite (Marsh, 1988; Higgins, 2017; Cashman, 2020).

In this study, the CL observation and CSD measurement of the three granitic rock samples collected from the well WD-1a were conducted in order to elucidate the solidification process of the granitic magma chamber from a petrographic point of view at the Kakkonda geothermal field.

2. Overview of the Kakkonda geothermal field

Geothermal power plants with a total capacity of 80 MWe are in operation at the Kakkonda geothermal field, northeast Japan (Fig. 1). The geology of the field was summarized by Kato *et al*. (1993), Kato and Sato (1995) and Doi *et al*. (1998). The basement of the field is the Pre-Paleogene (expressed "Pre-Tertiary" in the above papers) formation composed of slate, sandstone and andesitic tuff (Fig. 2). The Neogene formations are composed mainly of andesitic to dacitic tuff, tuffaceous sandstone and black shale. The Pleistocene rhyolitic to dacitic welded tuffs unconformably overly the Neogene formations. The Pleistocene-Holocene andesitic volcanic rocks cover the welded tuffs. The Pliocene dacitic intrusions are found in the Neogene rocks, and the Quaternary Kakkonda granite intruded the Pre-Paleogene and Neogene rocks.

Petrography and mineralogy of the Kakkonda granite were investigated by Kanisawa *et al*. (1994), Kato and Sato (1995) and Doi *et al*. (1998). It is made up of granodiorite, tonalite, quartz diorite and granite, and consists of fine to medium size crystals. The granitic magma began to be crystallized at 869-874 °C with suspension of basic clots based on the pyroxene geothermometer, and was solidified at 640-780 °C

based on the hornblende-plagioclase geothermometer and homogenization temperature of melt inclusion in quartz (Kanisawa *et al*., 1994; Sasaki *et al*., 2003). The granitic rocks showed the K-Ar ages of 0.24-0.11 Ma for hornblende, 0.21-0.02 Ma for biotite, and 0.14-0.01 Ma for K-feldspar (Kanisawa *et al*., 1994; Doi *et al*., 1998; Ito *et al*., 2013), and the values became younger at deeper depths.

Contact metamorphic aureole with a 1 km thickness occurs above the Kakkonda granite. Metamorphic minerals identified are biotite, cordierite, anthophyllite, orthopyroxene, clinopyroxene, and andalusite with small amounts of corundum, spinel, and K-feldspar (Kato and Sato, 1995; Sawaki *et al*., 2001). Metamorphic temperatures were estimated to be about 400 °C for biotite, 490 °C for cordierite, 570 °C for andalusite, and 600-700 °C for corundum based on the paragenesis of the metamorphic minerals and thermodynamic calculation (Sawaki *et al*., 2001; Takeno *et al*., 2001).

Geothermal fluid in the Kakkonda system circulates in the shallow and deep reservoirs, where the former has temperatures of 230-260 °C at depths of <1,500 m, and the latter has temperatures of 300-350 °C at depths of 1,500-3,100 m (Hanano and Takanohashi, 1993; Ikeuchi *et al*., 1998). The reservoirs are under the hydrothermal convection, while the granite distributed below a 3,100 m depth is under the thermal conduction with a steep gradient of 32 °C/100 m. Geothermal fluid in the hydrothermal convection zone is meteoric in origin and dilute, while fluid in the thermal conduction zone is magmatic in origin and hypersaline over a salinity of 40 wt.% with abundant CO_2 and H_2S gases and metal elements (Yanagiya *et al*., 1996; Kasai *et al*., 1998; Yanagisawa *et al*., 2002). Hydrothermal veins and fractures commonly occur in both the reservoirs with a high density, while they are sparse in the thermal conduction zone (Kato *et al*., 1998).

3. Description of core samples

The deep geothermal research well WD-1a encountered the granitic body at the 2,860 m depth, and drilled to the 3,729 m depth (Uchida *et al*., 1996; Muraoka *et al*., 1998; Saito *et al*., 1998). The well retrieved three spot-core samples of C11, C12 and C13 at depths of 2,938, 3,230 and 3,729 m at formation temperatures of 370 °C, 410 °C and 500-510 °C, respectively (Doi *et al*., 1998; Ikeuchi *et al*., 1998; Muraoka *et al*., 1998; Saito *et al*., 1998; Sasaki *et al.*, 2020).

Petrography and mineralogy of the samples were examined by Doi *et al*. (1998), Sasaki *et al*. (2003) and Nakano *et al*. (2014). C11 is granodiorite with weakly porphyritic texture, and has miarolitic cavities of about 5 mm in diameter (Ohtani *et al*., 2000). C12 is tonalite with granophyric texture. C13 is tonalite with equigranular texture, and remains free interstitial spaces (Fujimoto *et al*., 2000b). These granitic rocks are mainly composed of plagioclase, quartz, hornblende, and biotite with a small amount of K-feldspar. C11 and C12 have weakly undergone the metamorphism (Doi *et al.*, 1998). A quartz vein less than 1 cm in width occurs in C12, and a quartz vein less than 2 cm in width is found in C13.

Plagioclase occurs as euhedral to subhedral grains, and consists of irregular-shaped core with patchy zoning and mantle with oscillatory zoning. The mantle is surrounded by albite-rich rims in C11 and C12, but not in C13. K-feldspar occurs as interstitial grains, and exhibits perthite by exsolution of albite lamellae in C11 and C12, but not in C13. Quartz occurs as coarse to fine anhedral grains, and contains many fluid inclusions. Quartz in C13 incudes tiny unidentified minerals and melt inclusions in addition to the fluid inclusions. Hornblende occurs as euhedral to anhedral grains in C11 and C12 and subhedral to anhedral grains in C13. Biotite occurs as coarse platy grains, and sparsely as fine flaky grains in C11 and C12.

Orthopyroxene and clinopyroxene are only found as inclusions in plagioclase and hornblende.

In the previous works (Doi *et al*., 1998; Sasaki *et al*., 2003; Nakano *et al*., 2014), the presence of less- or non-altered constituent minerals such as K-feldspar without perthite, melt inclusion in quartz, and free interstitial space was identified as the petrographic feature of the high-temperature granite.

4. CL observation

Thin sections of the granitic rock samples were observed using a Nuclide® luminoscope at the Research Center of the Japan Petroleum Exploration Co. Ltd. under the operation conditions of acceleration voltage of 10 kV, excitation current of 0.8 mA, ambient pressure of 10-30 Pa under an atmosphere of He gas, and defocused area of 5x5-15x15 mm^2. The CL photomicrographs were taken with a Fuji ISO 400 film at various exposure times from several seconds to several minutes (Figs 3, 4, and 5).

Plagioclase, K-feldspar and quartz in the samples exhibited CL emission, but biotite and hornblende did not (Fig. 3a). The plagioclase showed CL color of bright yellow at the core, pale yellow, green or blue at the mantle, and pink to red at the rim in C11 and orange at the rim in C12 and C13. The K-feldspar showed CL color of bright blue. The quartz showed CL color of blue, purple, and dark red, and exhibited the following primary and secondary CL textures.

Quartz in C11 and C12 commonly showed monotone blue to purple CL color, but rarely displayed the following primary internal textures: a round-shaped core in relatively dark red color, only found in coarse grains (Fig. 3b); step zoning in transitional blue to dark red color, whose intervals were from 50 to 200 μm (Figs 3c, 3d); and smudged heterogeneity in blue or dark red color in coarse grains. Referring

previous works, the round-shaped core indicates the resorption of pre-existing quartz (D'Lemos *et al*., 1997; Müller *et al*., 2000; Peppard *et al*., 2001), and the step zoning (which is the gapped zoning with a >50 μm width relative to oscillatory zoning with a 2-20 μm width) implies the crystal growth with a change in physicochemical condition of magma. (Watt *et al*., 1997; Müller *et al*., 2000). Coarse quartz in C13 consisted of four zones (Fig. 3e): an irregular-shaped core in bright blue color (Q1), its surround in dark red to purple color (Q2), inner part adjacent to the grain edges in bright blue color (Q3), and the outermost part in dark red color (Q4). The Q1 zone contained many tiny unidentified minerals and melt inclusions. The Q3 zone commonly contacted with the mantle of plagioclase with pale blue color (arrow X in Fig. 3e), while the Q4 zone contacted with the rim of plagioclase with orange color (arrow Y in Fig. 3e). Fine quartz in C13 commonly exhibited twice zoning by repeats of blue to dark red color (Figs 3e and 4c), indicating the repeated resorption and overgrowth. Coarse quartz in C11 rarely showed the rounded shapes (Fig. 3f). These lines of observation revealed that quartz grew at three stages, distinguished by resorbed core, overgrown main body (rarely with step zoning), and repeatedly resorbed and overgrown periphery (or fine grains).

Quartz veins in C12 and C13 showed dark red CL color (Figs 4a and 4c). The vein in C12 cut coarse quartz and plagioclase in the host rock, but the vein quartz had the similar crystallographic orientations to the host quartz (Figs 4a and 4b). The vein in C13 appear to be continuous to the rims of the host quartz in CL color (Fig. 4c). Some coarse quartz consisted of fine grains with same crystallographic directions (Fig. 4d), implying aggregation and coalescence of the fine grains.

Quartz commonly exhibited many irregularly branched or curved lines under the CL observation (Fig. 5). They were less than several tens of microns in width, and had a close relation to the alignment of fluid inclusions and tiny unidentified minerals, implying either origin of healed microfracture, recrystallized region, or alteration halo,

with reference to the previous works (Sprunt and Nur, 1979; Valley and Graham, 1996; Van den Kerkhof and Hein, 2001). The areas of the lines in several individual quartz grains ranged from 3 to 34 % on the photomicrographs (Table 1). Fluid inclusion itself exhibited no CL emission.

5. Chemical analysis of quartz

In general, CL emission of the felspar group is attributed to the intrinsic trace impurities (Mn^{2+} for yellow to green, Ti^{4+} for blue, and Fe^{3+} for red), while that of quartz is due to a variety of factors such as trace impurities (Ti^{4+} and Mn^{2+} for blue and Al^{3+}, Na^{+} and water species for red), defects in crystal lattice, and mechanical deformation (Marshall, 1988; Walker and Burley, 1991; D'Lemos *et al*., 1997; Seyedolali *et al*., 1997). Chemical composition of quartz in the studied samples was preliminarily examined for major elements using an electron probe microanalyzer (JEOL JXA 8800R) at the Geological Survey of Japan (GSJ) with the analytical conditions of acceleration voltage of 15 kV, current emission of $1.2x10^{-8}$ A, counting time of 20 s and correction method of Bence and Albee (1968), and water species using a Nicolet 550 Magna IR FT-IR spectroscopy with a NicPlan IR microscope at the GSJ with the analytical conditions of measured area of 20x20–52x52 μm^2, scan range of 450-6,000 cm^{-1}, and scan time of 100 at a scan rate of 50 scan/min. The object of the FT-IR micro spectroscopy was coarse quartz in doubly polished thin section with 80-300 μm thickness, that was measured by a micro slide caliper with an accuracy of ±1 μm.

Quartz contained small amounts of Al and Ti (Table 2). They were abundant at the main bodies with blue CL color compared to the peripheries with red CL color. An application of the Ti geothermometer of Wark and Watson (2006) indicated

formation temperatures of 836-903 °C and 700-735 °C at the former and latter parts, respectively, suggesting that magma decreased in temperature during the crystallization of quartz.

Quartz showed four sharp peaks at 3,482, 3,433, 3,380 and 3,312 cm^{-1} in wavenumber in the FT-IR analysis (Fig. 6a). They were assigned to Al^{3+} substituting Si^{4+} with the charge balanced by H^{+} and alkali-metal cations (Li^{+} and Na^{+}) according to Aines and Rossman (1984). The noisy peaks in wavenumber higher than 3,600 cm^{-1} were due to influence of air during the analysis. Molecular water generally exhibits a broad peak around 3,400 cm^{-1} in wavelength (Aines and Rossman, 1984; Kronenberg and Wolf, 1990), but was not clearly recognized in this study except parts with visible fluid inclusion. Water contents were however hypothetically determined using the height of absorbance around 3,400 cm^{-1} in wavelength, as shown in Fig. 6a. The determination followed the Lambert-Beer law with a molar adsorption coefficient of 8.1 L mol^{-1} mm^{-1} (Aines and Rossman, 1984). The water contents determined were between 30 and 100 ppm at parts in clear quartz without visible fluid inclusion nor tiny mineral. The values were lower than those at parts in dusty quartz and quartz with visible fluid inclusions (Fig. 6b). The values were higher than the water contents in pure quartz (several ppm: Paterson, 1986), and were lower than those in deformed and metamorphosed quartz (several thousand ppm: Nakashima *et al*., 1995).

6. CSD measurement

CSD of plagioclase and quartz found in thin sections of the granitic rock samples were determined according to Marsh (1988). The photomicrographs taken under the optical microscopy were digitalized (Fig. 7a), and the crystals more than 0.1 mm in size at least were picked up with its check under the optical microscopy. The

areas of crystals were measured using a free software of ImageJ build at the National Institutes of Health, USA, in which the Analyze Particle command was available. The sizes of crystals were expressed as diameters of circles with areas equivalent to the measured values. The granitic rocks studied exhibited the 0.51-0.56 and 0.26-0.28 area % of plagioclase and quartz on the digitalized photomicrographs of the thin sections, respectively (Fig. 7a). The numbers of crystals per unit area on the thin sections were converted to the numbers of crystals per unit volume of the rocks through raising to 3/2 power, and the population density of crystals, that is the number of crystals in a given crystal-size class per unit volume, was determined (Fig. 7b). The population density generally obeys the following equation (Marsh, 1988):

$$n = n_0 \exp (-L / G\tau)$$

where n is the population density, n_0 is the nucleation density, L is the crystal size, G is the crystal growth rate, and τ is the crystal resident time. The $G\tau$ is the characteristic length of the crystal.

Numbers counted on each thin section of C11, 12, and 13 (Fig. 7a) were 3,060, 2219, and 1,269 for plagioclase and 2,568, 994, and 750 for quartz, respectively. Plagioclase and quartz showed convex shapes in the population density curves (Fig. 7b), with peaks at crystal sizes (critical sizes) of 0.2-0.3 mm in C11 and C12 and 0.3-0.4 mm in C13. The curves were almost linear above the critical sizes, and appear to obey the CSD theory. The linear intervals were relatively large in plagioclase compared to quartz. The curves below the critical sizes exhibited positive slopes, possibly due to sorption and annealing of the fine crystals (Ostwald ripening); this effect appears to become intense from C11 through C12 to C13. The n_0 and $G\tau$ values were determined by fitting the above-mentioned equation (Table 3). The n_0 and $G\tau$ values systematically decrease and increase, respectively, with samples from C11 through C12 to C13.

7. Numerical simulation on cooling of magma

Solidification duration of magma is one of the most important parameters to influence on the petrographic texture of the solidified immobile rigid crust (Marsh, 1989; 1996). Numerical simulations in previous works indicated various solidification durations for the Kakkonda granitic magma: 0.03-0.04 Ma (Muraoka and Matsubaya, 1994), 0.01 Ma (Hanano, 1998), 0.20 Ma (Shigeno, 2000), and 0.04-0.06 Ma (Ehara *et al*., 2001). Solidification duration at each depth of core sampling in the well WD-1a was determined in this study using an analytical solution of one-dimensional conductive heat flow between two contact blocks with different temperatures (Carslaw and Jaeger, 1959):

$$(Tm(d, t) - Tr_0) / (Tm_0 - Tr_0) = 1/2 (1 + erf (d / (2 \sqrt{k t})))$$

where Tm (d, t) is the temperature of magma at depth d and time t, Tm_0 is the initial temperature of magma with an infinite thickness downward, Tr_0 is the initial temperature of roof rock with an infinite thickness upward, and k is the thermal diffusivity. Solidification durations at the depths of C11, C12 and C13 were determined to be about 520, 11,700 and 64,500 years, respectively, at the initial conditions of Tm_0=1,000 °C, Tr_0=100 °C, and k=0.01 cm^2/s with solidification of magma at 700 °C (Fig. 8). These values were almost concordant to the previous works, and became to be longer at deeper depths.

The calculation, however, never attained the present-day temperatures in a reasonable duration because of the too gradual decrease in temperature below 600 °C. It should be then emphasized here that the formation of hydrothermal convection at the shallow depths forced the cooling of the granitic body, and consequently made the present-day thermal conduction zone with a steep gradient (32 °C/100 m: Ikeuchi *et al.*, 1998) at deep depths inside the granitic body.

8. Discussions

The following petrographic features were identified in the Kakkonda granitic rocks in this study: (i) porphyritic texture with miarolitic cavities in C11 contrastive to the equigranular texture with free interstitial spaces in C13, (ii) crystal growth of quartz occurring at three stages (implied from the resorbed core, overgrown main body, and repeatedly resorbed and overgrown periphery), (iii) solidification duration of magma being slow in order with depth in the numerical simulation, and (iv) plagioclase and quartz indicating the decrease in nucleation density (n_0) and increase in characteristic length ($G\tau$) with depth. Formation of these petrographic features during the cooling of magma and sequential granite was discussed below (Fig. 9).

8.1 Primary textures during the cooling of magma

Marsh (1989; 1996) defined the rigid crust as a crystallinity of >0.55, mush as 0.25 to 0.55, and suspension as <0.25. The granitic rocks studied exhibited the area % of 51-56 and 26-28 for plagioclase and quartz on the digitalized photomicrographs, respectively (Fig. 7a). Then, plagioclase was possible to form a crystal network of the rigid crust by itself, but its timing and quartz contribution to the network might differ from the margin inward the granitic body as follows. The solidification duration of magma became to be longer at deeper depths in the numerical simulation (Fig. 8). It is one of the key reasons for the formation of porphyritic texture in C11 contrastive to the equigranular texture in C13. This difference in texture should be ascribed into details by the nucleation and growth rates of crystals in magma. Regarding the solidification durations of magma determined in the simulation to the crystal resident time (τ) in magma, the crystal growth rate (G) and nucleation rate (J), that is defined by $J=n_0G$ in

the CSD theory (Marsh, 1988), were possibly calculated (Table 3). The G and J values of plagioclase and quartz systematically decrease with depth from C11 through C12 to C13. In C11, the G and J values of plagioclase were both faster than those of quartz, possibly forming a network of plagioclase crystals in magma followed by filling of interstitial spaces later with quartz crystals. These G and J values was fast enough to partially prevent the escape of aqueous fluid exsolved from the magma, resulting in the formation of miarolitic cavities. On the other hand, in C13, the G and J values of plagioclase and quartz were almost concordant to each other, possibly forming a texture composed equivalently of the plagioclase and quartz crystals, although the quartz occurred slightly behind the formation of the mantle of plagioclase (Fig. 3e). These G and J values of C13 slower than those of C11 remained only free interstitial spaces in the solidified rock, instead of the miarolitic cavities as like the C11. At the end during the solidification of magma, quartz repeatedly underwent the resorption and overgrowth, as recorded in the peripheries of coarse quartz and fine grains especially in C13 (Figs. 3e and 4c). It is attributed to the changes in physicochemical condition of residual magma such as temperature, pressure, and chemical composition. Then, the residual magma filled with the interstitial spaces was not so stagnant from a viewpoint of interaction with respect to quartz. The exsolution of aqueous fluid from the residual magma might also contribute to the changes in physicochemical condition of the residual magma.

8.2 Secondary textures during the cooling of granite

Two modifications of petrographic texture during the cooling of granite after the solidification of magma were recognized; they were the formation of perthite in K-feldspar with albitization of rims of plagioclase (Sasaki *et al*., 2003; Nakano *et al*., 2014), and healed microfractures in quartz inferred from the many branched and curved CL lines in this study (Fig. 5). The CL lines occupied large areas in individual quartz

crystals (Table 1). They might enlarge in appearance in a geological time because the diffusivity of water species in quartz is fast at high temperatures: in a case of oxygen parallel to the c-axes of quartz to be 0.37-3.26 μm/year at 450-600 °C and 0.44-4.55 μm/day at 700-900 °C (Giletti and Yund, 1984; Farver and Yund, 1991). The microfracturing of quartz is believed to provide a potential pathway for fluid and heat transfer in granite (Sprunt and Nur, 1979). Its effectiveness depends on the lifetime of microfractures in quartz. It has been examined in previous works to be less than a year at 300-400 °C and 100 MPa in a heating experiment of a granite (Moore *et al*., 1994) and less than 2 to 10 days at >550 °C and >50 MPa in a synthetic experiment of secondary fluid inclusions (Bodnar *et al*., 1985). Fluid inclusions in quartz of the Kakkonda granitic rocks showed homogenization temperatures of 350-550 °C mostly (Ikeuchi *et al*., 1998; Komatsu *et al*., 1998). Therefore, the microfractures identified in the studied quartz were never ceaseless, but taking into account of its number and areas, they might have provided an occasional pathway for fluid and heat transfer in a geological time. Thermal contraction of quartz (typically, α-β quartz transition) is a cause of the microfracturing of quartz in granite (Sprunt and Nur, 1979; Müller *et al*., 2002). However, the above-mentioned homogenization temperatures of fluid incisions in quartz of the Kakkonda granitic rocks were apparently lower than the α-β quartz transition temperature of 574 °C (Skinner, 1966), and rather indicate the microfracturing of quartz occurring with a relation to the formation of thermal conduction zone inside the granitic body. The Kakkonda granitic rocks remained the free interstitial spaces of 2.2-3.5 vol.% (Fujimoto *et al*., 2000b). They were filled with saline aqueous fluid (Kasai *et al*., 1998), and had a fluid pressure of 50 MPa at the bottom level of the well WD-1a (Fujimoto *et al*., 2000a); the value was in a transition between the hydrostatic and lithostatic fluid pressures. The transition is also a result of the formation of the thermal conduction zone in the granitic body. The gradient in fluid pressure in the thermal conduction zone might support the upward migration of

aqueous fluid through the granitic body in a geological time, as well as the remained free interstitial spaces in the granitic body.

9. Conclusions

The deep-seated Kakkonda granite is the heat source of the Kakkonda geothermal field, northeast Japan. Three granitic rocks collected by the deep geothermal research well WD-1a were petrographically examined in order to understand the solidification process of the Kakkonda granitic magma chamber, for which the CL observation and CSD measurement of the rocks were performed in this study.

The results of this study presented the following knowledge on the solidification process of a granitic magma chamber. Solidification duration of magma was the most important factor for the formation of petrographic texture in granite. The duration affected the nucleation and growth rates of plagioclase and quartz. They became slow from the margin inward the Kakkonda granitic body, resulting in the formation of porphyritic texture with miarolitic cavities to equigranular texture with free interstitial spaces from the margin inward the granitic body. The crystal network of the rigid crust was formed predominantly by crystallization of plagioclase followed by crystallization of quartz at a shallow level, while it was formed equivalently by crystallization of both the plagioclase and quartz at a deep depth, based on the nucleation and growth rates of the minerals determined. Quartz in the granitic rocks consisted of the resorbed core, overgrown main body, and repeatedly resorbed and overgrown periphery, indicating crystal growth of quartz at three stages, in which the magma was interactive with respect to quartz due to the changes in physicochemical condition of the magma, especially at the end during the solidification of magma.

Quartz in the granitic rocks recorded many healed microfractures. They occurred mainly with a relation to the formation of the thermal conduction zone inside the granitic body. The microfractures might provide a sporadic pathway for fluid and heat transfer in the granitic body in a geological time.

The result of this study might be helpful for a better understanding of the solidification process of a granitic magma chamber emplaced at a shallow level in the crust.

Acknowledgement

This study was conducted in the "Deep-Seated Geothermal Resources Survey" project in FY1992-2000 at the Geological Survey of Japan (GSJ), collaborated with the New Energy and Industrial Technology Development Organization (NEDO) and the Japan Metals and Chemicals Co. Ltd. (JMC). The authors thank the NEDO for providing the core samples. The authors are very grateful to Drs. Doi, N., Kato, O., Kasai, K., and Komatsu, R. of the JMC Geothermal Engineering Co., Ltd. for providing information on the Kakkonda geothermal field. The authors also thank Dr. Yagi, M. of the Research Center of the Japan Petroleum Exploration Co. Ltd. and Drs. Tsukamoto, H., Saito, G., and Yanagisawa, N. of the GSJ for operation assistance of analysis apparatuses. The authors appreciate Drs. Ohtani, T., Shigeno, H., Tamanyu, S., Muraoka, H., Shinohara, H., Kazahaya, K., and Takagi, T. for useful discussions on the field, magma, and granite.

References

Aines, R. D. and Rossman, G. R. (1984) What in minerals? A peak in the infrared. *Journal of Geophysical Research*, **89**, 4059-4071.

Bence, A. E. and Albee, A. L. (1968) Empirical correction factors for electron microanalysis of silicate and oxides. *The Journal of Geology*, **76**, 382-403.

Bodnar, R. J., Burnham, C. W. and Sterner, S. M. (1985) Synthetic fluid inclusions in natural quartz. III. Determination of phase equilibrium properties in the system H_2O-NaCl to 1000°C and 1500 bars. *Geochimica et Cosmochimica Acta*, **49**, 1861-1873.

Carslaw, H. S. and Jaeger, J. C. (1959) *Conduction of heat in solids (2nd ed.)*. Clarendon, Oxford, 396p.

Cashman, K. V. (2020) Crystal size distribution (CSD) analysis of volcanic samples: advances and challenges. *Frontiers in Earth Sciences*, **8**, 291.

Doi, N., Kato, O., Ikeuchi, K., Komatsu, R., Miyazaki, S., Akaku, K. and Uchida, T. (1998) Genesis of the plutonic-hydrothermal system around Quaternary granite in the Kakkonda geothermal system, Japan. *Geothermics*, **27**, 663-690.

D'Lemos, R. S., Kearsley, A. T., Pembroke, J. W., Watt, G. R. and Wright, P. (1997) Complex quartz growth histories in granite revealed by scanning cathodoluminescence techniques. *Geological Magazine*, **134**, 549-552.

Ehara, S., Fujimitsu, Y., Yamakawa, S. and Baba, H. (2001) Development of a hydrothermal system by conductive cooling of the heat source - a case study of Kakkonda geothermal system, Japan -. *Journal of Geothermal Research Society of Japan*, **23**, 11-23 (in Japanese with English abstract).

Farver, J. R. and Yund, R. A. (1991) Oxygen diffusion in quartz: dependence on temperature and water fugacity. *Chemical Geology*, **90**, 55-70.

Fujimoto, K., Sasaki, M., Sawaki, T. and Yanagisawa, N. (2000a) Structure and evolution process of the Kakkonda geothermal system from the viewpoint of

water-rock interaction. *Report of Geological Survey of Japan*, no. 284, 105-116 (in Japanese with English abstract).

Fujimoto, K., Takahashi, M., Doi, N. and Kato, O. (2000b) High permeability of Quaternary granites in the Kakkonda geothermal area, northeast Japan. *Proceedings of World Geothermal Congress 2000*, 1139-1144.

Giletti, B. J. and Yund, R. A. (1984) Oxygen diffusion in quartz. *Journal of Geophysical Research*, **89**, 4039-4046.

Hanano, M. (1998) A simple model of a two-layered high-temperature liquid-dominated geothermal reservoir as a part of large-scale hydrothermal convection system. *Transport in Porous Media*, **33**, 3-27.

Hanano, M. and Takanohashi, M. (1993) Reviews of recent development of the Kakkonda deep reservoir, Japan. *Proceedings, 18th Workshop on Geothermal Reservoir Engineering*, *Stanford University, Stanford, California, January 26-28, 1993*, SGT-PR-145.

Higgins, M. D. (2017) Quantitative investigation of felsic rock textures using cathodoluminescence images and other techniques. *Lithos*, **277**, 259-268.

Ikeuchi, K., Doi, N., Sakagawa, Y., Kamenosono, H. and Uchida, T. (1998) High-temperature measurements in well WD-1a and the thermal structure of the Kakkonda geothermal system, Japan. *Geothermics*, **27**, 591-607.

Ito, H., Tamura, A., Morishita, T., Arai, S., Arai, F. and Kato, O. (2013) Quaternary plutonic magma activities in the southern Hachimantai geothermal area (Japan) inferred from zircon LA-ICP-MS U-Th-Pb dating methos. *Journal of Volcanology and Geothermal Research*, **265**, 1-8.

Kanisawa, S., Doi, N., Kato, O. and Ishikawa, K. (1994) Quaternary Kakkonda Granite underlying the Kakkonda geothermal field, northeast Japan. *Journal of Mineralogy Petrology and Economic Geology*, **89**, 390-407 (in Japanese with English abstract).

Kasai, K., Sakagawa, Y., Komatsu, R., Sasaki, M., Akaku, K. and Uchida, T. (1998) The origin of hypersaline liquid in the Quaternary Kakkonda Granite, sampled from well WD-1a, Kakkonda geothermal system, Japan. *Geothermics*, **27**, 631-645.

Kato, O. and Sato, K. (1995) Development of deep-seated geothermal reservoir bringing the Quaternary granite into focus in the Kakkonda geothermal field, northeast Japan. *Resource Geology*, **45**, 131-144 (in Japanese with English abstract).

Kato, O., Doi, N. and Muramatsu, Y. (1993) Neo-granitic pluton and geothermal reservoir at the Kakkonda geothermal field, Iwate prefecture, Japan. *Journal of Geothermal Research Society of Japan*, **15**, 41-57 (in Japanese with English abstract).

Kato, O., Doi, N., Sakagawa, Y. and Uchida, T. (1998) Fracture systematics in and around well WD-1, Kakkonda geothermal field, Japan. *Geothermics*, **27**, 609-629.

Komatsu, R., Ikeuchi, K., Doi, N., Sasaki, M., Uchida, T. and Sasada, M. (1998) Characteristics of the Quaternary Kakkonda Granite and geothermal system clarified by fluid inclusion study of deep investigation well, Kakkonda, Japan. *Journal of Geothermal Research Society of Japan*, **20**, 209-224 (in Japanese with English abstract).

Kronenberg, A. and Wolf, G. H. (1990) Fourier transform infrared spectroscopy determinations of intragranular water content in quartz-bearing rocks: implication for hydrolytic weakening in the laboratory and within the earth. *Tectonophysics*, **172**, 255-271.

Marsh, B. D. (1988) Crystal size distribution (CSD) in rocks and the kinetics and dynamics of recrystallization I. Theory. *Contributions to Mineralogy and Petrology*, **99**, 277-291.

Marsh, B. D. (1989) Magma chamber. *Annual Review of Earth and Planetary Science*, **17**, 439-474.

Marsh, B. D. (1996) The 1995 Hallimond Lecture Solidification fronts and magmatic evolution. *Mineralogical Magazine*, **60**, 5-40.

Marshall, D. J. (1988) *Cathodoluminescence of Geological Materials*. Unwin Hyman, London, 146p.

Moore, D. E., Lockner, D. A. and Byerlee, J. D. (1994) Reduction of permeability in granite at elevated temperatures. *Science*, **265**, 1558-1561.

Müller, A., Seltmann, R. and Behr, H.-J. (2000) Application of cathodoluminescence to magmatic quartz in a tin granite - case study from the Schellerhau granite complex, Eastern Erzgebirge, Germany. *Mineralium Deposita*, **35**, 169-189.

Müller, A., Lennox, P. and Trzebski, R. (2002) Cathodoluminescence and micro-structural evidence for crystallization and deformation processes of granites in the Eastern Lachlan Fold Belt (SE Australia). *Contributions to Mineralogy and Petrology*, **143**, 510-524.

Muraoka, H. and Matsubaya, O. (1994) Estimation of magma chamber size from the thickness of contact metamorphic aureoles. *Memoir of Geological Society of Japan*, no. 43, 73-86 (in Japanese with English abstract).

Muraoka, H., Uchida, T, Sasada, M., Yagi, M., Akaku, K., Sasaki, M., Yasukawa, K., Miyazaki, S., Doi, N., Saito, S., Sato, K. and Tanaka, S. (1998) Deep geothermal resources survey program: igneous, metamorphic and hydrothermal processes in a well encountering 500 °C at 3,729 m depth, Kakkonda, Japan. *Geothermics*, **27**, 507-534.

Nakano, S., Sawaki, T. and Sasaki, M. (2014) Microtexture and compositional variation of alkali feldspars from the Kakkonda granitic pluton, northeast Japan: implications to the formation processes of granitic texture. *Journal of Mineralogical and Petrological Sciences*, **109**, 138-150.

Nakashima, S., Matayoshi, H., Yuko, T., Michibayashi, K., Masuda, T., Kuroki, N., Yamagishi, H., Ito, Y. and Nakamura, A. (1995) Infrared microspectroscopy analysis of water distribution in deformed and metamorphosed rocks. *Tectonophysics*, **245**, 263-276.

Ohtani, T., Nakashima, Y. and Muraoka, H. (2000) Three-dimensional miarolitic cavity distribution in the Kakkonda granite from borehole WD-1a using X-ray computerized tomography. *Engineering Geology*, **56**, 1-9.

Paterson, M. S. (1986) The thermodynamics of water in quartz. *Physics and Chemistry of Minerals*, **13**, 245-255.

Peppard, B. T., Steele, I. M., Davis, A. M., Wallace, P. J. and Anderson, A. T. (2001) Zoned quartz phenocrysts from the rhyolitic Bishop Tuff. *American Mineralogist*, **86**, 1034-1052.

Saito. S., Sakuma, S. and Uchida, T. (1998) Drilling procedures, techniques and test results for a 3.7 km deep, 500 °C exploration well, Kakkonda Japan. *Geothermics*, **27**, 573-590.

Sasaki, M., Sawaki, T. and Sakaguchi, K. (2020) Photographs of the core samples taken from the deep exploration well WD-1. *Open-File Report of Geological Survey of Japan, AIST*, no. 696, 49p (in Japanese).

Sasaki, M., Fujimoto, K., Sawaki, T., Tsukamoto, H., Kato, O., Komatsu, R., Doi, N. and Sasada, M. (2003) Petrographic features of a high-temperature granite just newly solidified magma at the Kakkonda geothermal field, Japan. *Journal of Volcanology and Geothermal. Research*, **121**, 247-269.

Sawaki, T., Sasaki, M., Fujimoto, K., Takeno, N., Tsukamoto, H., Sanada, K. and Maeda, S. (2001) Corundum and zincian spinel from the Kakkonda geothermal system, Iwate Prefecture, northeastern Japan. *Journal of Mineralogical and Petrological Sciences*, **96**, 137-147.

Seyedolali, A., Krinsley, D. H., Boggs, Jr. S., O'Hara, P. F., Dypvik, H. and Goles, G. G. (1997) Provenance interpretation of quartz by scanning electron microscope - cathodoluminescence fabric analysis. *Geology*, **25**, 787-790.

Shigeno, H. (2000) Evolution history of the Kakkonda magma hydrothermal system, Japan, estimated through simplified model numerical simulations. *Proceedings, 25th Workshop on Geothermal Reservoir Engineering, Stanford University, Stanford, California, January 24-26, 2000*, SGP-TR-165.

Skinner, B. J. (1966) Thermal expansion. *In* Clark, Jr., S. P. ed., *Handbook of Physical Constants*, Geological Society of America Memoir, **97**, 75-96.

Sprunt, E. S. and Nur, A. (1979) Microcracking and healing in granites: new evidence from cathodoluminescence. *Science*, **205**, 496-497.

Takeno, N., Muraoka, H., Sawaki, T. and Sasaki, M. (2001) Thermodynamic framework of the contact metamorphism around the Kakkonda granite in an active geothermal field, northeast Japan. *Proceedings of 10th International Symposium Water-Rock Interaction* (R. Cidu, ed.), vol. 1, 765-768.

Tsukamoto, H. (1994) Geological application of luminescent microscopy and spectroscopy. *Chishitsu News*, no. 474, 46-56 (in Japanese).

Uchida, T., Akaku, K., Sasaki, M., Kamenosono, H., Doi, N. and Miyazaki, S. (1996) Recent progress of NEDO's "Deep-Seated Geothermal Resources Survey" project. *Geothermal Resources Council Transaction*, **20**, 643-648.

Valley, J. W. and Graham, C. M. (1996) Ion microprobe analysis of oxygen isotope ratios in quartz from Skye Granite: healed micro-cracks, fluid flow, and hydrothermal exchange. *Contributions to Mineralogy and Petrology*, **124**, 225-234.

Van den Kerkhof, A. M. and Hein, U. F. (2001) Fluid inclusion petrography. *Lithos*, **55**, 27-47

Walker, G. and Burley, S. (1991) Luminescence petrography and Spectroscopic studies of diagenetic minerals. *In* Barker, C. E. and Kopp, O. C., eds., *Luminescence and Microscopy: qualitative and quantitative application*, SEPM short course, **25**, 83-96.

Wark, D. A., and Watson, E. B. (2006) TitaniQ: a titanium-in-quartz geothermometer. *Contributions to Mineralogy and Petrology*, **152**, 743-754.

Watt, G. R., Wright, P., Galloway, S. and Maclean, C. (1997) Cathodoluminescence and trace element zoning in quartz phenocrysts and xenocrysts. *Geochimica et Cosmochimica Acta*, **61**, 4337-4348.

Yanagisawa, N., Fujimoto, K. and Hishi, Y. (2002) Scale variation of the production wells from deep reservoir in Kakkonda field. *Proceedings, 27th Workshop on Geothermal Reservoir Engineering, Stanford University, Stanford, California, January 28-30, 2002*, SGT-PR-171.

Yanagiya, S., Kasai, K., Brown, K. L. and Giggenbach, W. F. (1996) Chemical characteristics of deep geothermal fluid in the Kakkonda geothermal system, Iwate prefecture, Japan. *Journal of Japan Geothermal Energy Association*, **33**, 1-18 (in Japanese with English abstract).

Yuguchi, T., Ogita, Y., Kato, T., Yokota, R., Sasao, E. and Nishiyama, T. (2020) Crystallization processes of quartz in a granitic magma: cathodoluminescence zonation pattern controlled by temperature and titanium diffusivity. *Journal of Asian Earth Sciences*, **192**, 104289 (https://doi.org/10.1016/j.jseaes.2020.104289).

Tables

Table 1 Areas of the CL lines identified in quartz on the photomicrographs.

Samples	Area %					
C11	14.53	15.07	12.29	15.17	17.51	-
C12	3.84	22.58	34.03	17.83	33.27	18.92
C13	16.70	11.00	22.41	21.68	18.63	-

Table 2 Chemical composition of quartz in C13.

No.	SiO_2	Al_2O_3	TiO_2	Na_2O	K_2O	CaO	MgO	FeO	MnO	Total	T. (^oC)
main bodies with blue CL color											
9	99.29	0.03	0.05	0.02	-	-	-	-	-	99.40	903
10	99.83	0.01	0.03	0.02	0.01	-	-	0.05	0.01	99.95	836
peripheries with red CL color											
11	99.11	0.01	0.02	0.01	-	0.00	-	0.08	0.01	99.23	735
12	99.06	0.002	0.01	-	0.02	-	-	0.08	-	99.17	700

Note, T.(^oC): calculated by the Ti geothermometer of Wark and Watson (2006).

Table 3 Parameters of the CSD theory determined in this study.

Samples		Ln (n_0) (/mm^4)	Gτ (mm)	τ (yr)*	G (mm/s)	J (N/mm^3 s)
Pl	C11	4.1	0.17	520	1.0E-11	6.5E-10
	C12	4.0	0.17	11700	4.5E-13	2.4E-11
	C13	2.8	0.21	64500	1.0E-13	1.6E-12
Qz	C11	5.4	0.10	520	6.4E-12	1.3E-09
	C12	2.5	0.16	11700	4.3E-13	5.2E-12
	C13	2.2	0.21	64500	1.0E-13	9.5E-13

Note: n_0, nucleation density; G, crystal growth rate; τ, crystal resident time; J, crystal nucleation rate; and *, determined in Fig. 8.

Figures

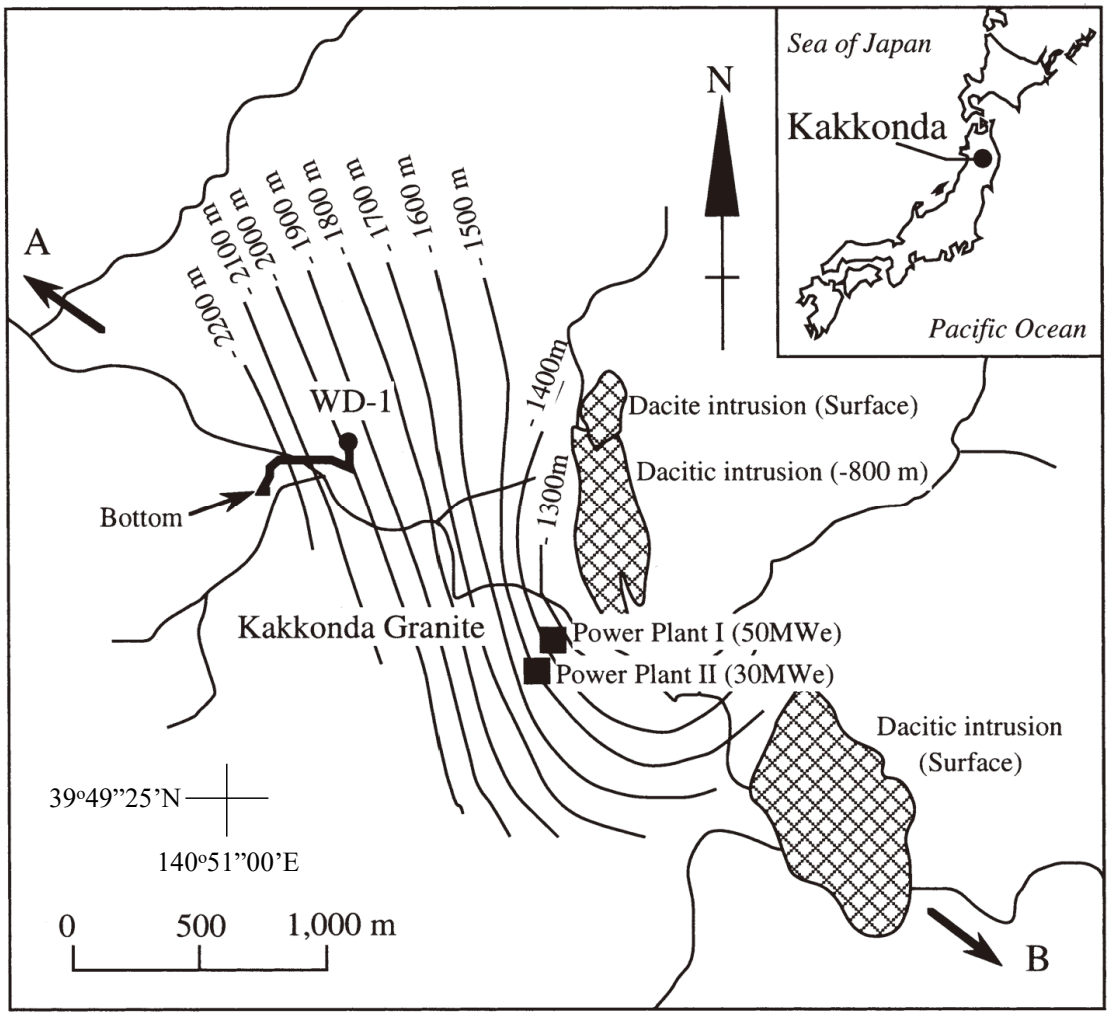

Fig. 1 Locality of the Kakkonda geothermal field, northeast Japan (modified after Kato and Sato, 1995 and Doi *et al*., 1998). The contours indicate the top of the Kakkonda granitic body (in relation to the sea level). Arrows with "A" and "B" correspond to the cross section in Fig. 2.

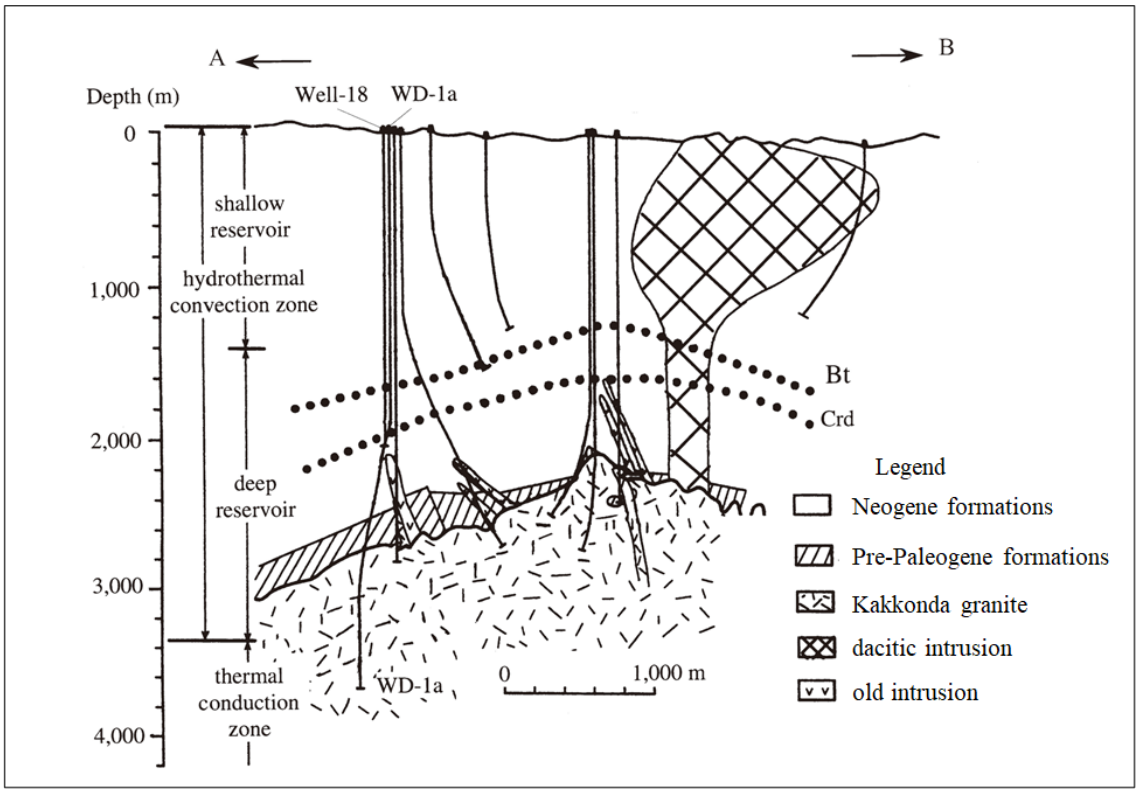

Fig. 2 A cross-section of the Kakkonda geothermal field, corresponding to the A-B line in Fig. 1 (simplified after Kato *et al*., 1993 and Doi *et al*., 1998). Abbreviations of Bt and Crd indicate the shallowest appearance depths of the metamorphic biotite and cordierite, respectively.

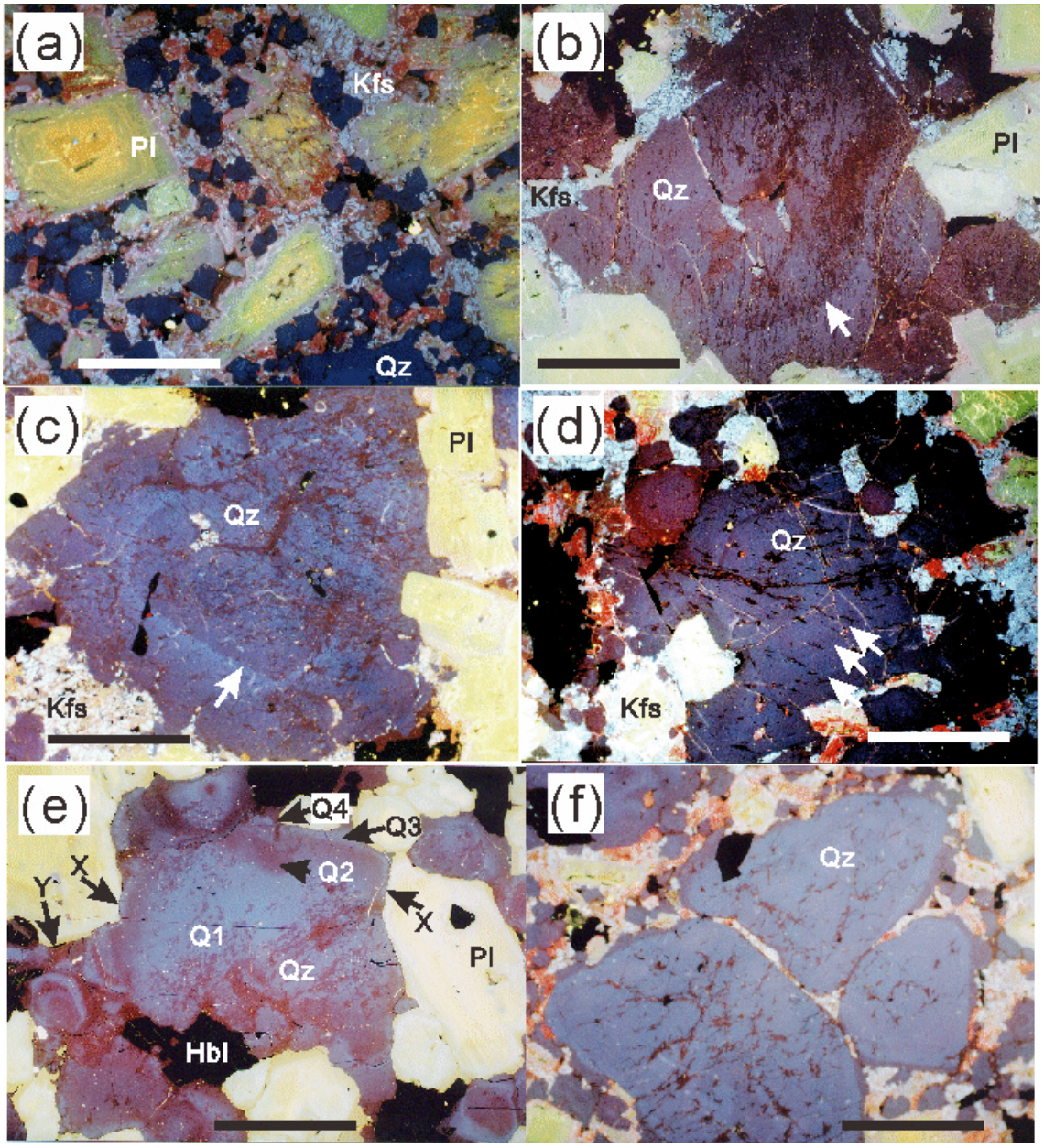

Fig. 3 CL photomicrographs of the primary petrographic textures.

(a) plagioclase showing CL colors in yellow at its core, green at its mantle, and red at its rim, K-feldspar in bright blue, and quartz in dark blue to purple (C11). (b) Coarse quartz having a round-shaped core in dark red CL color (arrow) and many irregularly branched and curved CL lines in dark red color (C12). (c) Coarse quartz with step zoning in a transitional CL color from blue to dark red (arrow) (C12). (d) Coarse quartz with step zoning (arrows) (C11). (e) Coarse quartz consisting of four zones (C13): an irregular-shaped core in bright blue

color (Q1), its surround in dark red to purple color (Q2), inner part adjacent to the grain edges in bright blue color (Q3), and the outermost part in dark red color (Q4), in which the Q3 zone contacts with the mantles of plagioclase in pale blue CL color (arrow “X”) and the Q4 zone contacts with the outermost parts of plagioclase in orange CL color (arrow “Y”). (f) Coarse quartz exhibiting round shapes (C11). Abbreviations: Hbl, hornblende; Kfs, K-feldspar; Pl, plagioclase; and Qz, quartz. Scale bar: 1 mm.

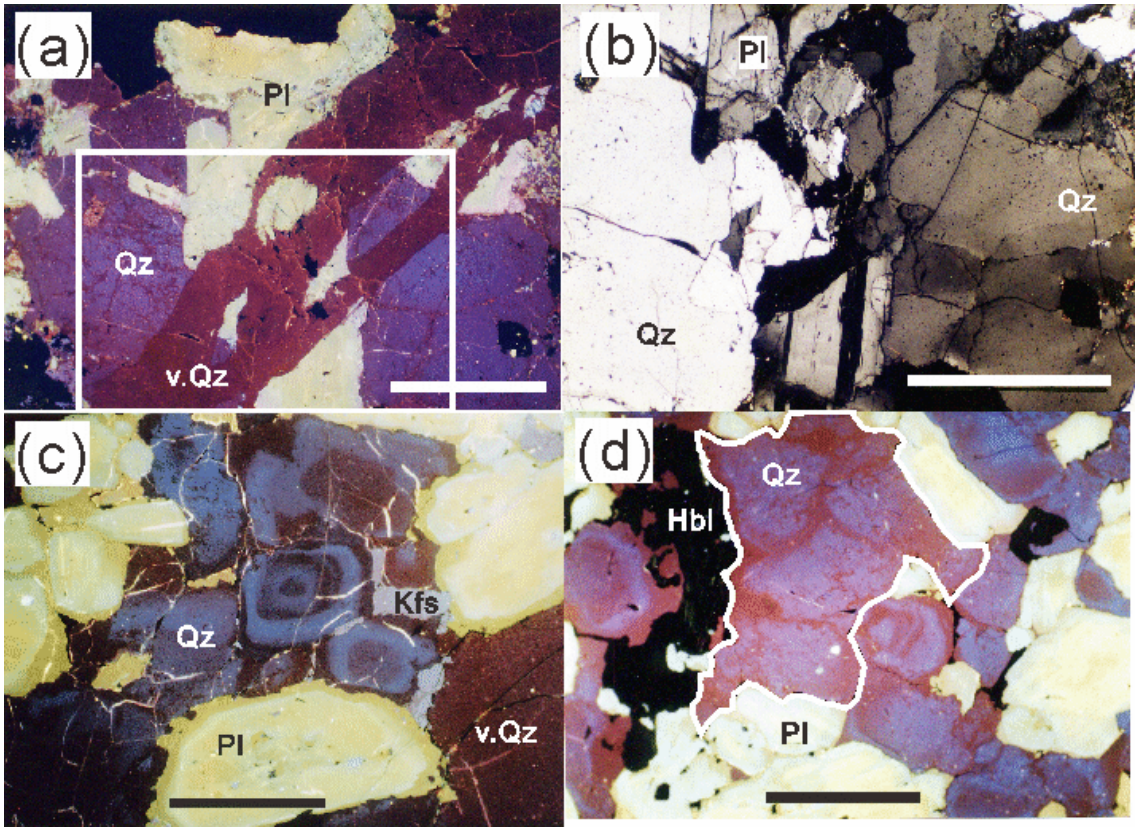

Fig. 4 CL photomicrographs of the secondary petrographic textures.

(a) quartz vein cutting the host coarse quartz and plagioclase (C12). Square part enlarged in Fig. 4b. (b) quartz vein in the square part of Fig. 4a taken under the optical microscopy in the crossed-nicol state, where the vein and host quartz have same crystallographic directions. (c) a contact part between quartz vein and host rock in (C13), where the vein and outermost parts of host quartz shows a same CL color. (d) coarse quartz composed of fine grains with same crystallographic directions (surrounded by a white marker) (C13). Abbreviations: Kfs, K-feldspar; Pl, plagioclase; and Qz, quartz; and v.Qz, vein quartz. Scale bar: 1 mm.

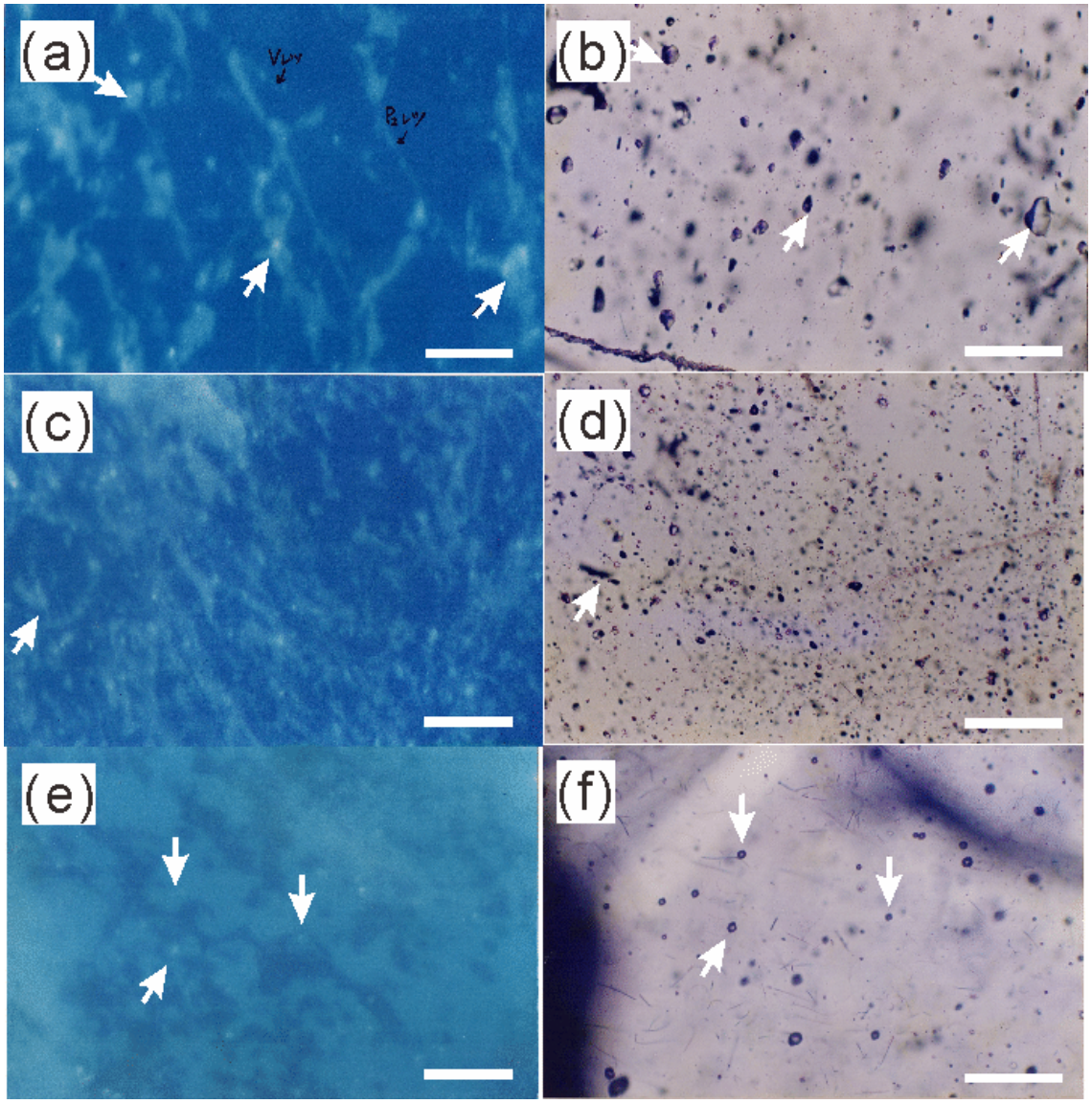

Fig. 5 CL and optical photomicrographs of the quartz in left and right sides, respectively.

(a) and (b) C11, (c) and (d) C12, and (e) and (f) C13. Arrows indicate fluid inclusions. Scale bar: 0.1 mm. The CL emission was observed using a JSM-6300 scanning electron microprobe attached an optical microscopic window and a cooling stage (Tsukamoto, 1994) under operation conditions of acceleration voltage of 30 kV, excitation current of 2-20 μA, stage temperature of –194 °C, ambient pressure of 6.6×10^{-4} Pa, and defocused area of 0.01x0.01-0.12x0.18 cm^2, and was taken with Fuji ISO 1600 films at various exposure times.

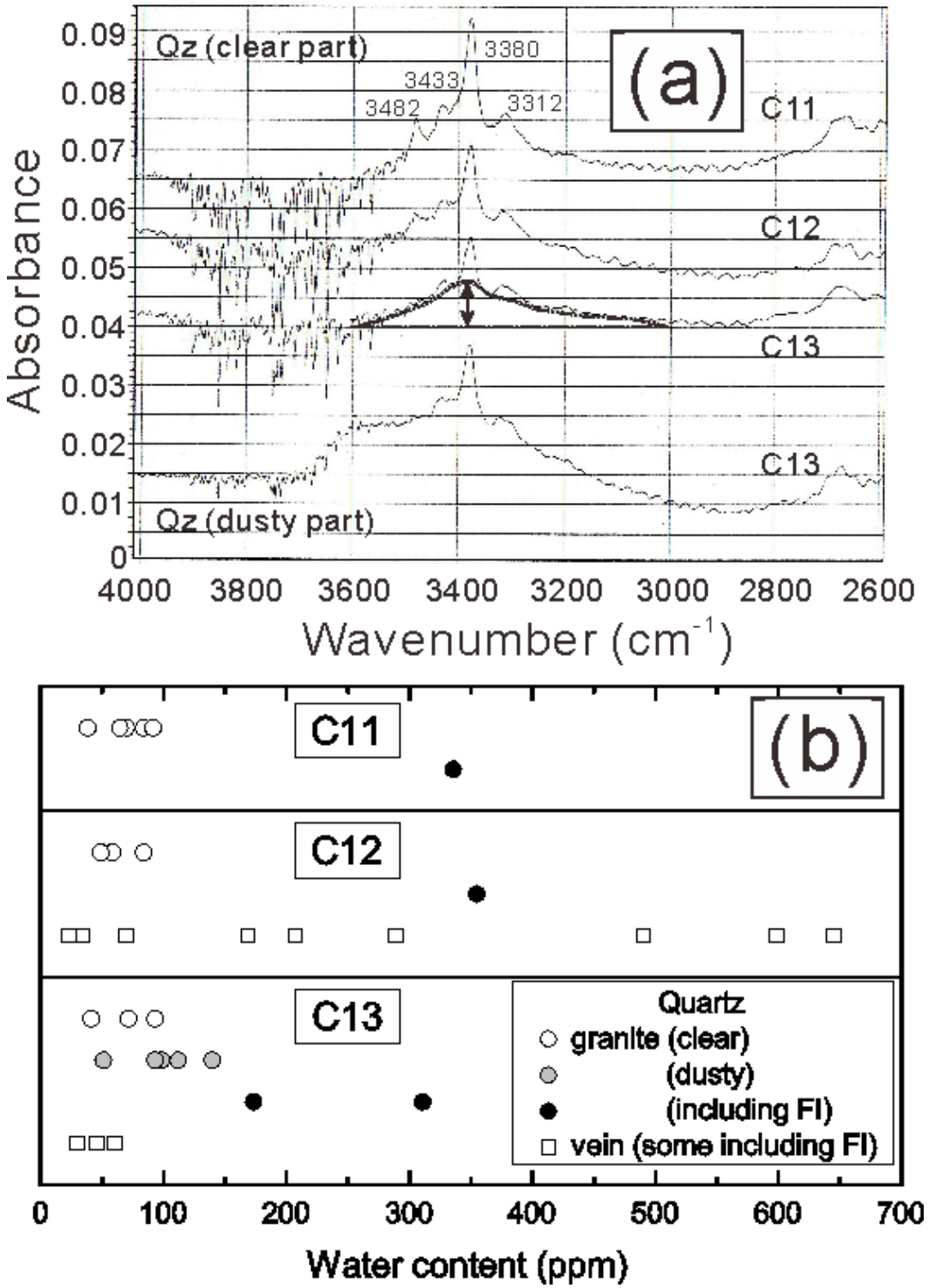

Fig. 6 Result of the micro FT-IR analysis of quartz.

(a) absorbance in wavenumber. Arrow indicates a height of absorbance around 3,400 cm^{-1}, which was used for the calculation of water content in quartz. (b) water contents at various parts in quartz. The term "FI" means fluid inclusion.

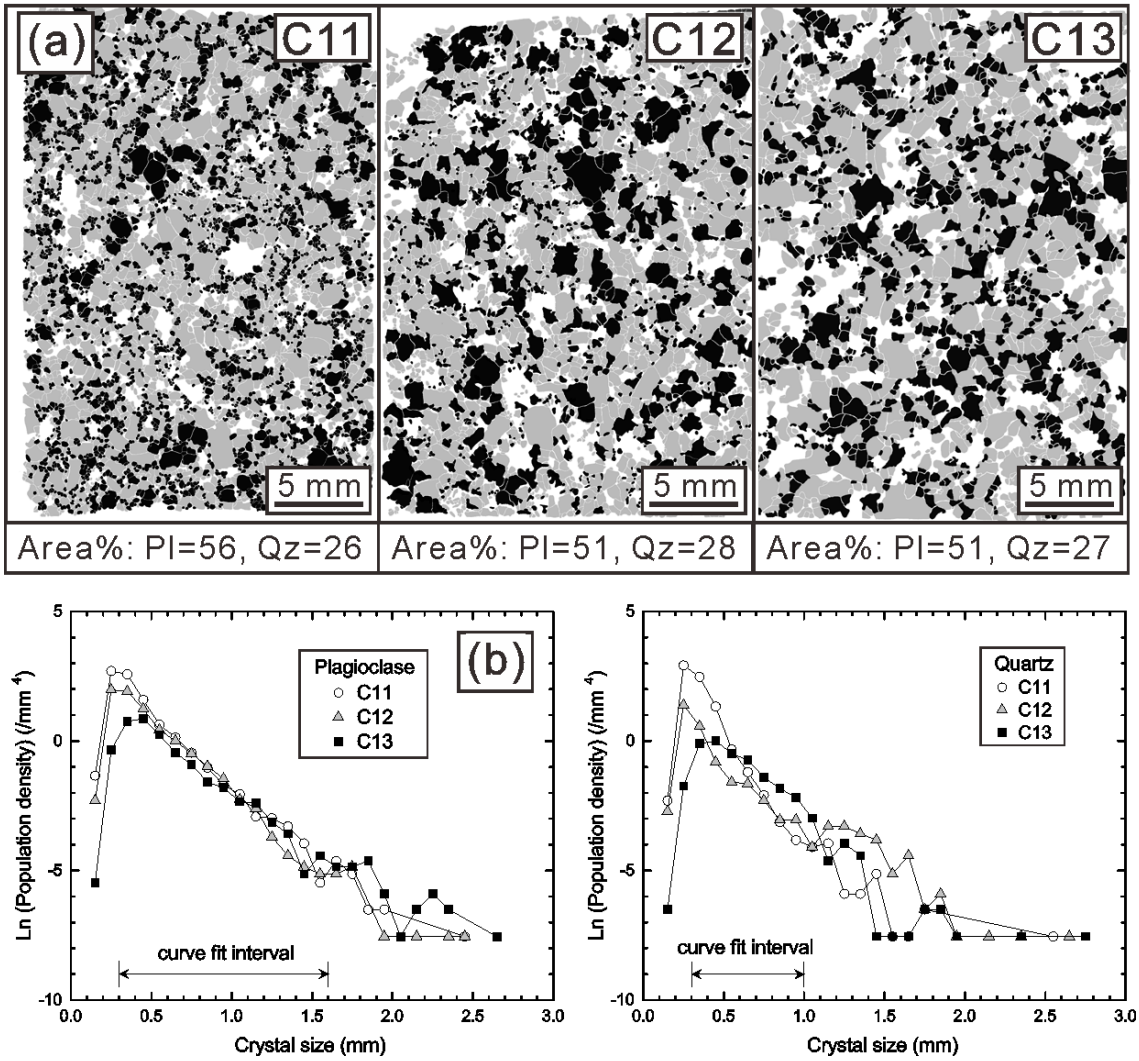

Fig. 7 Result of the CSD measurement.

(a) digitalized images of thin sections (gray: plagioclase, black: quartz). (b) population density curves of plagioclase and quartz.

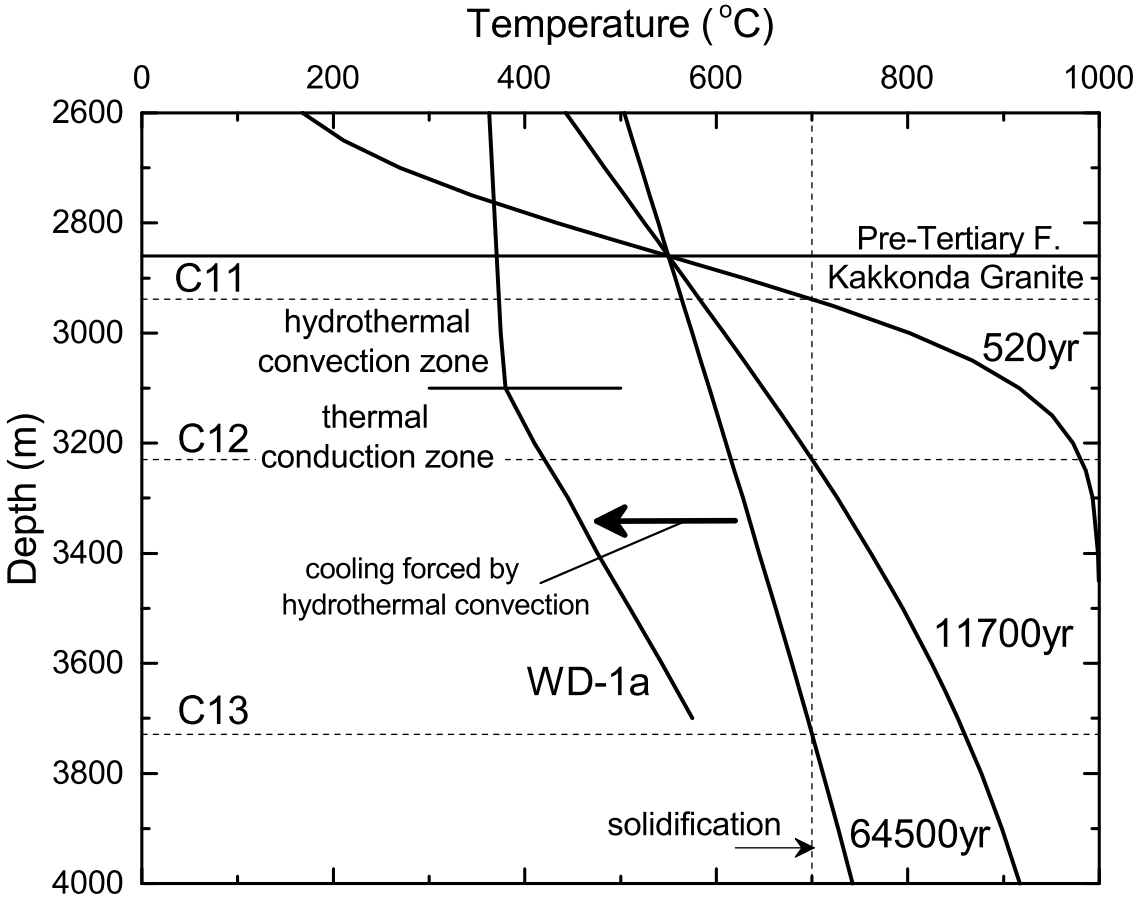

Fig. 8 Thermal profiles of a cooling magma determined through a numerical simulation, whose initial calculation conditions were in the context.

Temperature profile of the well WD-1a was cited from Ikeuchi *et al*. (1998).

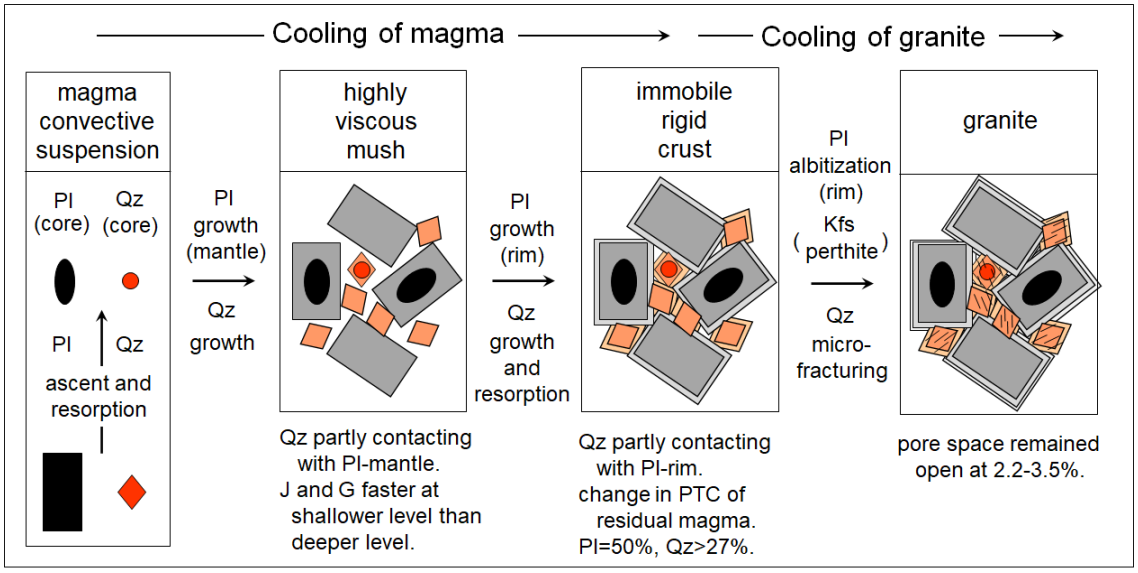

Fig. 9 Schematic formation of petrographic texture during cooling of the magma and sequential granite for the Kakkonda granite.

Citation:

Sasaki, M., Sawaki, T., Fujimoto, K. and Sasada, M. (2022) Petrographic texture of quartz in the Kakkonda granite, northeast Japan. Open-File Report of Geological Survey of Japan, AIST, no. 735, 36p.